Ultramicroscopy 109 (2009) 338–343

Contents lists available at ScienceDirect

Ultramicroscopy

journal homepage: www.elsevier.com/locate/ultramic

Probe retrieval in ptychographic coherent diffractive imaging

Pierre Thibault [a,*], Martin Dierolf [a,b], Oliver Bunk [a], Andreas Menzel [a], Franz Pfeiffer [a,b]

[a] Paul Scherrer Institut, 5232 Villigen PSI, Switzerland
[b] École Polytechnique Fédérale de Lausanne, 1015 Lausanne, Switzerland

ARTICLE INFO

Article history:
Received 25 September 2008
Received in revised form
4 December 2008
Accepted 23 December 2008

PACS:
42.30.Rx
42.30.Va
42.30.Kq
42.15.Dp

Keywords:
Phase retrieval
Ptychography
Diffractive imaging
Difference map algorithm

ABSTRACT

Ptychography is a coherent diffractive imaging method that uses multiple diffraction patterns obtained through the scan of a localized illumination on the specimen. Until recently, reconstruction algorithms for ptychographic datasets needed the *a priori* knowledge of the incident illumination. A new reconstruction procedure that retrieves both the specimen's image and the illumination profile was recently demonstrated with hard X-ray data. We present here the algorithm in greater details and illustrate its practical applicability with a visible light dataset. Improvements in the quality of the reconstruction are shown and compared to previous reconstruction techniques. Implications for future applications with other types of radiation are discussed.

1. Introduction

Most coherent diffractive imaging (CDI) methods rely on far-field diffraction data to retrieve the complex-valued projection or three-dimensional density of a sample. Unless the sample is periodic, as is the case in crystallography, finite coherence length and fixed dimensions of the detector pixels impose a limit on the amount of information carried by the wave for the problem to be tractable. For this reason, all CDI techniques require "oversampling" of the diffraction pattern, i.e. that the region in real-space contributing to the diffraction data does not extend beyond a limit predefined by the experimental conditions. In many experiments, oversampling is achieved with a plane wave incident on an isolated specimen. Despite the successes of this approach [1–4], the requirement for sufficiently small and isolated samples is an important obstacle to a wider application of the technique.

To overcome the isolated specimen limitation, one has to depart from the special case of planar incident waves, and rather select a region of the specimen with the illumination itself, either with a mask or a focused beam. This experimental convenience can however lead to insurmountable reconstruction difficulties. Propagation effects produce illuminated regions with smooth edges—a situation documented as hard, if not impossible to treat in the traditional reconstruction schemes [5]. In certain situations, the problem can still be solved if the wavefield incident on the specimen is also well known. This so-called "key-hole CDI" was demonstrated recently [6,7].

Data analysis can be further eased if redundancy in the data is introduced through multiple measurements with different but partly overlapping illuminated regions. This concept, called "ptychography", was introduced nearly 40 years ago for applications in electron microscopy [8]. Ptychography was recently reformulated to be used with a simpler and efficient iterative reconstruction algorithm [9] whose potential was demonstrated lately with visible light [10] and X-rays [11].

Using hard X-rays, it was recently demonstrated that both the specimen's transmission function and the illumination profile can be extracted from a ptychographic dataset [12]. In this article, we describe in greater details the reconstruction approach, and demonstrate its possibility with a laser light experiment. Our algorithm is based on the difference map, a general algorithm that solves constraint-based problems. It differs from another recently published method [13] that also addresses the probe retrieval problem. After describing the algorithm and addressing the question of uniqueness of the solution, we will present the reconstruction results and discuss the implications of the ability to retrieve the illumination profile for future applications of ptychography.

* Corresponding author. Tel.: +41 56 310 3705.
E-mail address: pierre.thibault@psi.ch (P. Thibault).

0304-3991/$ - see front matter © 2009 Elsevier B.V. All rights reserved.
doi:10.1016/j.ultramic.2008.12.011

2. Reconstruction algorithm

Detailed descriptions of ptychography can be found in a number of earlier publications [14,15]. A specimen is illuminated with a finite and coherent incident wave called the "probe". The wave emerging from the specimen propagates to the far field, where a pixel-array detector measures its intensity. A complete dataset consists of a set of such diffraction patterns, each corresponding to a known displacement of the probe relative to the specimen. Hence, one has

$$I_j(\mathbf{q}) = |\mathscr{F}[P(\mathbf{r}-\mathbf{r}_j)O(\mathbf{r})]|^2, \tag{1}$$

where I_j is the jth measured diffraction pattern, P is the probe function, O is the specimen's transmission function (the object) and $\mathscr{F}$ denotes the Fourier transform operation, with the reciprocal space coordinate $\mathbf{q}$. Reconstruction of the image amounts to recovering a function O that satisfies (1) for all j's.

Early solutions of ptychographic problems where obtained with a method called "Wigner deconvolution" [14]. Simultaneous reconstruction of the object and the probe functions was attempted in this formalism [16], in which it becomes a blind deconvolution problem. Although very elegant, Wigner deconvolution requires that the probe positions $\mathbf{r}_j$ lie on a grid as fine as the aimed resolution, making it impractical in many situations.

More recently, Rodenburg and Faulkner [9] have introduced an iterative reconstruction algorithm inspired from other commonly used phase retrieval algorithms, such as Fienup's hybrid input–output [17]. Called "ptychographic iterative engine" (PIE), the algorithm cycles through all datasets sequentially to update the object function. The algorithm bears some resemblance with a general form described by Youla [18] and Flåm [19] for convex set feasibility problems, every step being viewed as an under-relaxed projection. While its formulation is natural and intuitive, it is unclear how PIE can be generalized to allow the simultaneous reconstruction of the probe with the object.

The reconstruction procedure described in this paper departs from both previously known methods. It uses the difference map [20], an iterative algorithm originally devised for phase retrieval but now known to have a much wider range of applications [21]. The algorithm is designed to solve problems that can be expressed as the search for the intersection point between two constraint sets. Incidentally, the ptychographic problem (1) can be re-expressed trivially as two intersecting constraints by introducing the exit waves $\{\psi_j\}$ (the "views" on the specimen) corresponding to each position of the probe on the specimen. The Fourier constraint expresses compliance to the measured intensities,

$$I_j = |\mathscr{F}\psi_j|^2, \tag{2}$$

and the overlap constraint states that each view can be factorized as a probe and an object function:

$$\psi_j(\mathbf{r}) = P(\mathbf{r}-\mathbf{r}_j)O(\mathbf{r}). \tag{3}$$

This reformulation is the crucial step in the design of our reconstruction method. It fundamentally entails choosing a high-dimensional Euclidean space to embed the two constraint sets. This search space, in which iterations will take place, is the direct product of the spaces of each individual views. A state vector can then be written as $\Psi = (\psi_1(\mathbf{r}), \psi_2(\mathbf{r}), \ldots, \psi_N(\mathbf{r}))$. After this choice of model, subsequent calculations are dictated by the difference map formalism. The algorithm requires distance-minimizing projections onto the constraint sets. These operations modify minimally an input state vector Ψ to make it satisfy a given constraint.

The projection associated to the Fourier constraint Π_F simply consists in applying the Fourier projection, denoted by p_F, on each individual view:

$$\Pi_F(\Psi) : \psi_j \to \psi_j^F = p_F(\psi_j). \tag{4}$$

Given an estimate ψ_j of the jth view, $p_F(\psi_j)$ is obtained by replacing the magnitudes of the Fourier transform by $\sqrt{I_j}$ while keeping the original phases. This operation, not always called a projection, is ubiquitous in iterative phase retrieval methods in imaging and crystallography (see for instance Ref. [22]).

The overlap projection can be computed from the minimization of the distance $\|\Psi - \Psi^O\|^2$, subject to the constraint (3). The calculation entails to finding $\hat{O}$ and $\hat{P}$ that minimize

$$\|\Psi - \Psi^O\|^2 = \sum_j \sum_{\mathbf{r}} |\psi_j(\mathbf{r}) - \hat{P}(\mathbf{r}-\mathbf{r}_j)\hat{O}(\mathbf{r})|^2. \tag{5}$$

The associated projection is

$$\Pi_O(\Psi) : \psi_j \to \psi_j^O(\mathbf{r}) = \hat{P}(\mathbf{r}-\mathbf{r}_j)\hat{O}(\mathbf{r}). \tag{6}$$

Minimization of Eq. (5) must be carried numerically as closed form expressions for $\hat{O}$ and $\hat{P}$ cannot be obtained. For this task, various methods such as conjugate gradients minimization can be used efficiently. In particular, line minimization of (5) involves only finding the root of a polynomial of order 3. Alternatively, setting to zero the derivative of $\|\Psi - \Psi^O\|^2$ with respect to $\hat{P}$ and $\hat{O}$ gives the solution as a system of equations

$$\hat{O}(\mathbf{r}) = \frac{\sum_j \hat{P}^*(\mathbf{r}-\mathbf{r}_j)\psi_j(\mathbf{r})}{\sum_j |\hat{P}(\mathbf{r}-\mathbf{r}_j)|^2}, \tag{7}$$

$$\hat{P}(\mathbf{r}) = \frac{\sum_j \hat{O}^*(\mathbf{r}+\mathbf{r}_j)\psi_j(\mathbf{r}+\mathbf{r}_j)}{\sum_j |\hat{O}(\mathbf{r}+\mathbf{r}_j)|^2}. \tag{8}$$

In the event the probe $\hat{P}$ is already known, the overlap projection is given by (6), where $\hat{O}$ is computed with Eq. (7). If $\hat{P}$ also needs to be retrieved, both Eqs. (7) and (8) need to be simultaneously solved. While the system cannot be decoupled analytically, applying the two equations in turns for a few iterations was observed to be an efficient procedure to find the minimum. Within the reconstruction scheme, initial guesses for $\hat{P}$ and $\hat{O}$ are readily available from the previous iteration—apart from the very first iteration for which a rough model of the probe is needed to start the search for a minimum.

The reconstruction is implemented with the above projections, using the difference map. With a standard choice of parameters [20], the iterative procedure takes a form similar to Fienup's hybrid input–output algorithm [17],

$$\Psi_{n+1} = \Psi_n + \Pi_F[2\Pi_O(\Psi_n) - \Psi_n] - \Pi_O(\Psi_n). \tag{9}$$

Owing to the algorithm's very wide range of applications, it is doubtful that a general proof of convergence exists, as is the case for instance in the narrower case of projections on convex sets [18,23]. General properties of the algorithm have been studied in detail by Elser [24] and its converging behavior has been verified in multiple situations.

The initial state vector is typically generated with a random number generator, although transient time can be reduced with a better initial estimate of the views. In many cases, we have observed that setting the initial views equal to the starting guess of the probe improved convergence time by preventing the formation of phase vortices.

Iteration of Eq. (9) is carried until a fixed point is reached, i.e. $\Psi_{n+1} = \Psi_n$. The solution is then given by either the second or third term in Eq. (9), which are equal upon convergence. The quantities of interest are not the views but rather $\hat{O}$ and $\hat{P}$. These are readily computed during the evaluation of $\Pi_O(\Psi_n)$.

Convergence is monitored with the difference map error,

$$\varepsilon_{n+1} = \|\Psi_{n+1} - \Psi_n\|, \tag{10}$$

which gives an indication of the distance between the constraint sets in the vicinity of Ψ_n. In practice, because of noise and other experimental limitations, the constraint sets are never perfectly compatible. The iteration thus never comes to a halt, but reaches a steady state regime where the error is small but non-zero.

Another error metric, most commonly used in the crystallographic phase problem, is the "*R*-factor", traditionally written as

$$R = \frac{\sum_{\mathbf{q}} |F_{\mathrm{obs}}(\mathbf{q}) - F_{\mathrm{calc}}(\mathbf{q})|}{\sum_{\mathbf{q}} F_{\mathrm{obs}}(\mathbf{q})}. \tag{11}$$

In crystallography, F_{obs} are the observed Fourier amplitudes and F_{calc} are amplitudes obtained from an atomic model. In many CDI applications, *a priori* information is generally too scarce to define a model, and the *R*-factor loses its meaning. The high degree of redundancy in ptychographic datasets suggests that the significance of the *R*-factor is preserved, with Eq. (3) as the model. Eq. (11) then takes the form

$$R = \frac{\sum_{\mathbf{q},j} |\sqrt{I_j(\mathbf{q})} - |\mathscr{F}(P(\mathbf{r}-\mathbf{r}_j)O(\mathbf{r}))||}{\sum_{\mathbf{q},j} \sqrt{I_j(\mathbf{q})}}. \tag{12}$$

We note that recent simulations [13] indicate that a mere minimization of a cost function similar to Eq. (12) can converge to the sought solution.

As in many inverse problems, the question of uniqueness of the solution is critical in phase retrieval. Uniqueness can be compromised in two qualitatively different ways. First, as was just stated, noise and other experimental imperfections render the problem formally ill-defined: no state Ψ satisfies exactly both constraint sets. Fortunately, it is now known—at least empirically—that this rarely is a limitation. Reconstruction algorithms such as the difference map and the hybrid input–output share the important characteristic of being unstable if the constraint sets are too far away. Excessive noise or otherwise incompatible constraints therefore never lead to convergence. Other more rudimentary algorithms such as the error-reduction [17,25] do not exhibit this behavior, and convergence is generally not a sign of success. In most cases, if the steady state described above is reached, a convenient way of ensuring uniqueness of the reconstruction is to compute the average of many solution attempts from this final steady state.

The second threat to uniqueness can be more critical. It can be described as internal degrees of freedom that are not or very weakly constrained by the information available in the very problem formulation—thus independent of the reconstruction method. Some degrees of freedom are always present but nevertheless innocuous. Most of the time, a reconstructed image can be multiplied with an arbitrary phase factor $\exp(i\varphi)$ without harm. Similarly, any translation of the image is generally compatible with the measured data as well. Among more problematic cases is the presence of large regions of missing data in the diffraction patterns [26].

The approach described above makes apparent that the reconstruction of a ptychography dataset is equivalent to the simultaneous phase retrieval of multiple diffraction patterns. Provided that each diffraction pattern is sufficiently oversampled, conditions for the uniqueness of each of the views are the same as those defined in the phase retrieval of a single diffraction pattern [27]. An additional uncontrolled degree of freedom can however appear in the process of factorizing the views into *P* and *O*. Assuming that a solution to the problem (2)–(3) has been found, let two new functions be $O'(\mathbf{r}) = f(\mathbf{r})O(\mathbf{r})$ and $P'(\mathbf{r}) = [f(\mathbf{r})]^{-1}P(\mathbf{r})$. It can be seen that O' and P' are also solution of the problem if and only if

$$f(\mathbf{r}) = f(\mathbf{r}-\mathbf{r}_j) \quad \forall \mathbf{r}_j. \tag{13}$$

In the special (albeit common) case where the points $\mathbf{r}_j$ lie on a lattice, f can be any periodic function on this lattice. This infinite number of possible f translates into an infinity of possible solutions to the ptychographic problem. This "raster grid pathology" can be avoided with a different choice of probe positions to break the symmetry. With numerical simulations, we have found that artifacts from the use of a raster grid are mild in many cases because the probe positions are rounded to the nearest pixel values, thereby modulating slightly the otherwise perfect lattice.

3. Results

We have tested the reconstruction method described above on a dataset collected with laser light. The experimental setup, especially simple, is illustrated in Fig. 1. A 200 μm diameter pinhole was placed in the path of a HeNe laser beam. The specimen, an insect wing, was mounted on a translation stage and placed about 1 mm behind the pinhole. The detector, a CCD with

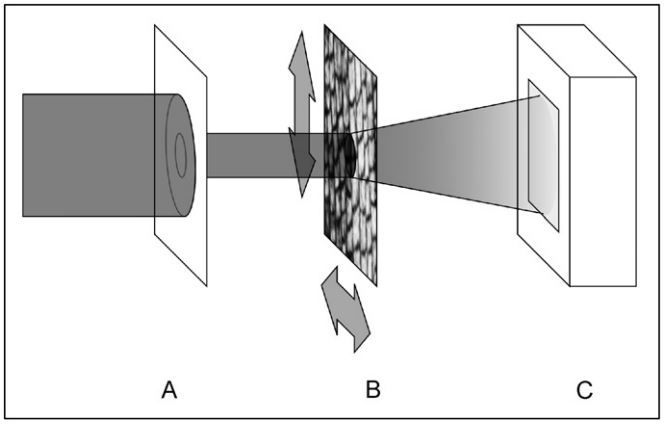

Fig. 1. Experimental setup. A portion of the incoming beam is selected with a pinhole (A). The wave at the exit of the pinhole propagates freely over a short distance before hitting the specimen (B). The resulting diffraction pattern is collected with a CCD detector (C).

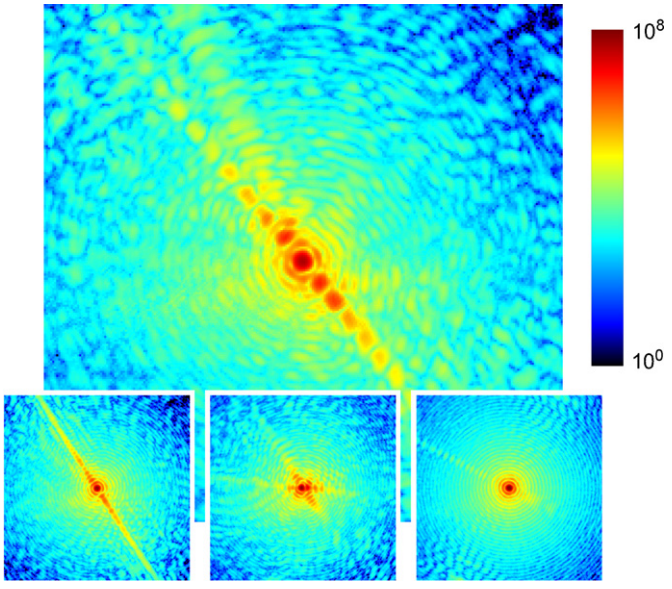

Fig. 2. Four of the 121 diffraction patterns used in the reconstruction (logarithmic scale). Each diffraction pattern is a combination of four exposures (0.3, 3, 15 and 30 s) to cover the dynamic range of about seven orders of magnitude. These datasets extend to spatial frequencies of about 100 μm^{-1}.

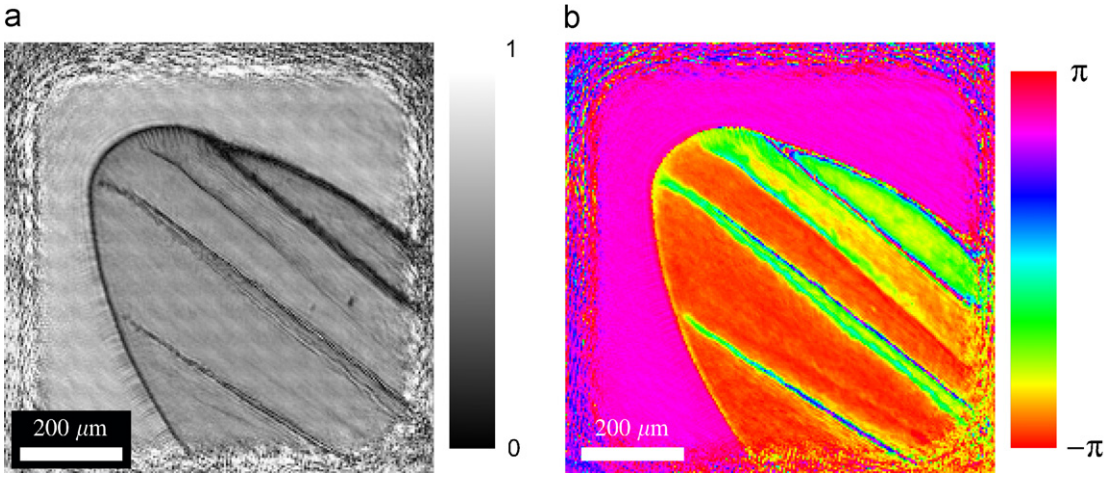

Fig. 3. (a) Amplitude and (b) phase of the reconstructed insect wing. Both quantities translate directly to the integrated complex index of refraction of the wing along the propagation direction.

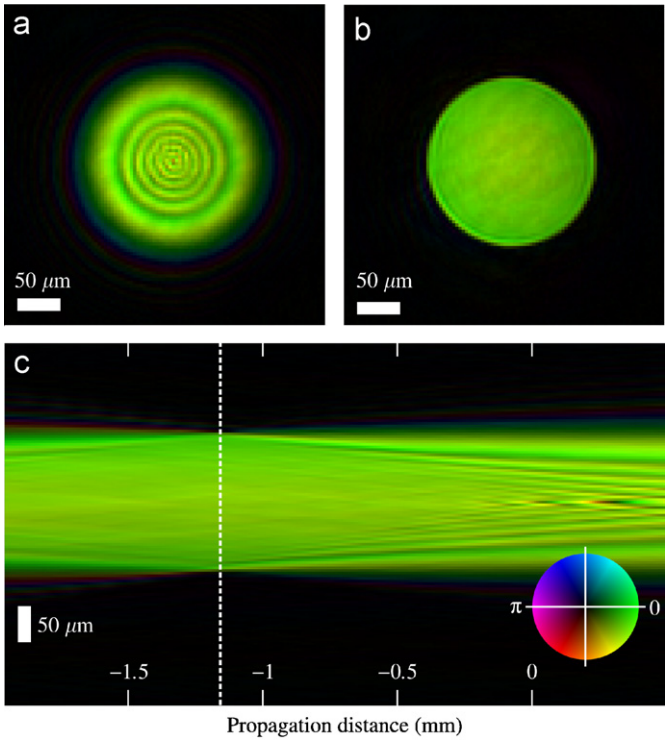

Fig. 4. Probe profile retrieved from the insect wing dataset. (a) Color rendering of the complex-valued reconstructed probe. The amplitude of the wavefield is mapped to the image brightness, and the phase is mapped to hue. (b) Computed free-space propagation of the reconstructed probe to a plane situated 1.19 mm upstream, where the pinhole was placed. A slight radial variation in hue shows the presence of a light curvature in the reconstructed wavefront. (c) Longitudinal cut of the propagated wavefield, showing clearly the waist of the wavefield in the pinhole plane.

24 μm pixel size, was placed 140 mm downstream to collect the diffraction pattern. Scattering angles up to 120 mrad in the corners could be collected, leading to a reconstruction pixel size of about 4 μm.

Examples of measured diffraction patterns are shown in Fig. 2. Information on the illuminated part of the specimen is encoded as a modulation of the Airy function profile from the pinhole. One important challenge in CDI experiments is the broad range of intensities that need to be detected; in the current experiment, up to seven orders of magnitude were recorded. The limited dynamic range of the CCD was overcome by a combination of multiple exposures. The complete dataset is a 11×11 raster grid with 50 μm step size.

The reconstructed image of a selected portion of the insect wing is shown in Fig. 3. As mentioned above, the complex-valued reconstruction carries both the absorption and the phase shift experienced by the wave as it traverses the specimen. Fig. 4a shows the complex-valued wavefield of the probe reconstructed along with the object's image. The concentric fringes in the probe profile can be at once identified as a Fresnel propagation effect. Knowledge of the full probe wavefield in a plane allows easy numerical propagation of the field back to the pinhole plane. Fig. 4b and c shows that the reconstructed wavefield is indeed consistent with a circular aperture placed upstream from the specimen. In particular, Fig. 4c can be used to deduce precisely the distance between the specimen and the pinhole.

4. Discussion

The reconstruction method introduced in this paper has multiple implications for the future of ptychography. The most straightforward consequence of simultaneous probe retrieval is an improvement in the image quality. Unknown imperfections of a fixed illumination have deteriorating effects on the reconstruction. This aspect is especially relevant for X-ray and electron diffraction, where an accurate model of the probe may be hard to obtain. This effect is illustrated in Fig. 5, where three reconstructions of the same dataset are compared. In addition to the current probe refinement scheme, two other reconstructions were produced using a modeled probe. One of these two reconstructions uses the PIE algorithm, while the other uses the difference map-based approach presented in this article, with the exception that only the object is updated at every iteration, i.e. P is kept constant instead of being refined with Eq. (8). For the two fixed-probe reconstructions, the model probe was defined as the wavefield emerging from a 200 μm circular aperture and propagated over a 1.1 mm distance, about 90 μm smaller than the value obtained with the back-propagation described above. Fig. 5a shows the R-factor of these reconstructions as a function of the iteration number. Both this graph and the images below clearly illustrate the gains in reconstruction quality. The figure also shows that both fixed probe techniques yield very similar reconstructions when provided with the same input information (diffraction data and model probe).

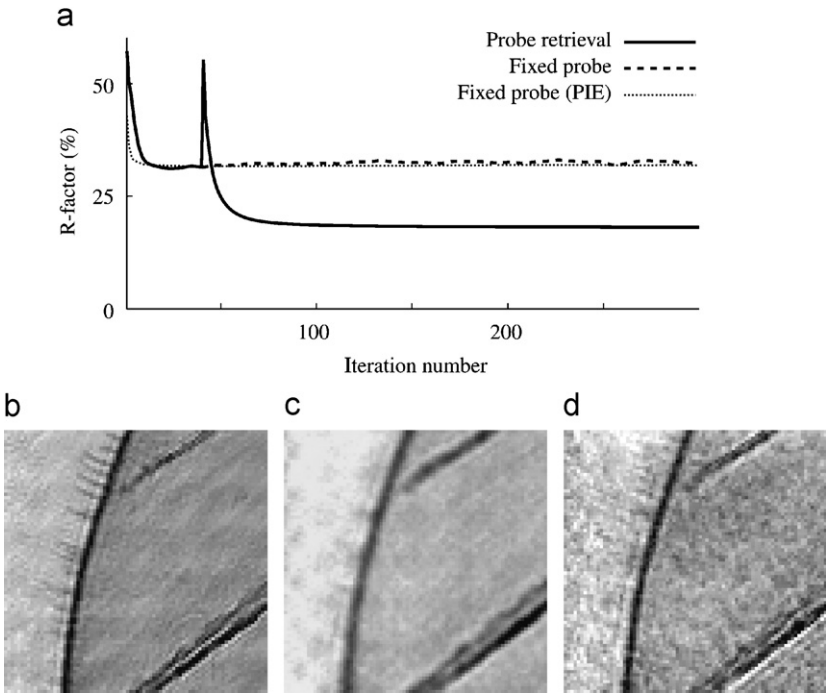

Fig. 5. Illustration of the probe retrieval performance. Imperfect modeling of the fixed probe is introduced by propagating the wavefield at the exit of a 200 μm pinhole over a distance of 1.1 mm, instead of 1.19 mm as was obtained from the analysis of the retrieved probe. (a) *R*-factor as a function of the iteration number. The probe retrieval was started after 40 iterations, resulting in a sudden increase of the *R*-factor, followed by a decrease to about 18% (compared with 32% for the two other reconstructions). (b)–(d) show a portion of the amplitude part of the reconstruction. The blurred appearance of the second image is explained by the averaging procedure, which PIE does not include, and suggests that the latter contains unreliable high-resolution features.

We note that the current approach is expected to work, without modification, with data obtained in other scattering geometries. For instance, within the paraxial approximation, it is well known that a near-field diffraction pattern is identical (up to rescaling) to the far-field diffraction pattern of the exit wave multiplied with a quadratic phase factor. Because it is multiplicative, this phase factor is automatically absorbed in the reconstructed probe, and the problem formulation remains unchanged. This property explains that the reconstruction presented in this article succeeds despite the relatively short distance between the specimen and the detector, giving a Fresnel number of about 0.5. A careful observation of the backpropagated probe actually shows a slight phase curvature. The measured curvature agrees to about 5% with the expected value given by the dimensions of the experiment. Following the same arguments, the reconstruction procedure is equally valid for data obtained with curved incident wavefronts [6,7].

Reconstructing both the object and the probe obviously requires more information than reconstructing the object alone. For instance, the "raster pathology" presented above dictates that the probe is never uniquely determined if a dataset is made of three diffraction patterns or less. The amount of overlap between neighboring illumination positions is important for the convergence rate of the PIE algorithm [28]. A similar behavior is expected for the algorithm presented in this paper. A thorough evaluation of these characteristics has yet to be done.

5. Summary and outlook

In this article, we have used a visible light ptychography experiment to demonstrate the capabilities of a new reconstruction algorithm. In addition to the complex-valued transmission function of the object, it was possible to retrieve from the data the complex wavefield incident on the specimen. We have shown that the probe retrieval procedure can improve noticeably the quality of the reconstruction. This feature is especially useful in X-ray or electron diffraction experiments, where predicting the incident wavefield can be otherwise very challenging.

Beyond image improvements, the method promises to be useful as a means to map the wavefront itself. A complete knowledge of the wavefield allows the investigation of the effect of optical components placed upstream. In the present report, a simple propagation calculation of the wavefield allowed to characterize the shape of the pinhole and its distance to the specimen. This wavefront sensing configuration is expected to be a powerful tool for the characterization of coherent X-ray optics in synchrotron sources or X-ray free-electron lasers.

References

[1] J. Miao, P. Charalambous, J. Kirz, D. Sayre, Extending the methodology of X-ray crystallography to allow imaging of micrometre-sized non-crystalline specimens, Nature 400 (1999) 342–344.
[2] G.J. Williams, M.A. Pfeifer, I.A. Vartanyants, I.K. Robinson, Three-dimensional imaging of microstructure in Au nanocrystals, Phys. Rev. Lett. 90 (175501) (2003) 1–4.
[3] D. Shapiro, P. Thibault, T. Beetz, V. Elser, M.R. Howells, C. Jacobsen, J. Kirz, E. Lima, H. Miao, A.M. Nieman, D. Sayre, Biological imaging by soft X-ray diffraction microscopy, Proc. Natl. Acad. Sci. USA 102 (43) (2005) 15343–15346.
[4] H.N. Chapman, A. Barty, S. Marchesini, A. Noy, C. Cui, M.R. Howells, R. Rosen, H. He, J.C.H. Spence, U. Weierstall, T. Beetz, C. Jacobsen, D. Shapiro, High-resolution *ab initio* three-dimensional X-ray diffraction microscopy, J. Opt. Soc. Am. A 23 (5) (2006) 1179–1200.
[5] J.R. Fienup, Reconstruction of a complex-valued object from the modulus of its Fourier transform using a support constraint, J. Opt. Soc. Am. A 4 (1) (1987) 118–123.
[6] G.J. Williams, H.M. Quiney, B.B. Dhal, C.Q. Tran, K.A. Nugent, A.G. Peele, D. Patterson, M.D. de Jonge, Fresnel coherent diffractive imaging, Phys. Rev. Lett. 97 (025506) (2006) 1–4.

[7] B. Abbey, K.A. Nugent, G.J. Williams, J. Clark, A.G. Peele, M.A. Pfeifer, M. de Jonge, I. McNulty, Keyhole coherent diffractive imaging, Nat. Phys. (4) (2008) 394–398.
[8] R. Hegerl, W. Hoppe, Dynamische Theorie der Kristallstrukturanalyse durch Elektronenbeugung im inhomogenen Primärstrahlwellenfeld, Ber. Bunsenges. Phys. Chem. 74 (1970) 1148–1154.
[9] J.M. Rodenburg, H.M.L. Faulkner, A phase retrieval algorithm for shifting illumination, Appl. Phys. Lett. 85 (2004) 4795–4797.
[10] J.M. Rodenburg, A.C. Hurst, A.G. Cullis, Transmission microscopy without lenses for objects of unlimited size, Ultramicroscopy 107 (2007) 227–231.
[11] J.M. Rodenburg, A.C. Hurst, B.R. Dobson, F. Pfeiffer, O. Bunk, C. David, K. Jefimovs, I. Johnson, Hard-X-ray lensless imaging of extended objects, Phys. Rev. Lett. 98 (034801) (2007) 1–4.
[12] P. Thibault, M. Dierolf, A. Menzel, O. Bunk, C. David, F. Pfeiffer, High-resolution scanning X-ray diffraction microscopy, Science 321 (2008) 379–382.
[13] M. Guizar-Sicairos, J.R. Fienup, Phase retrieval with transverse translation diversity: a nonlinear optimization approach, Opt. Express 16 (10) (2008) 7264–7278.
[14] J.M. Rodenburg, R.H.T. Bates, The theory of super-resolution electron microscopy via Wigner-distribution deconvolution, Phil. Trans. R. Soc. London A 339 (1655) (1992) 521–553.
[15] J.M. Rodenburg, Ptychography and related diffractive imaging methods, in: P. Hawkes (Ed.), Advances in Imaging and Electron Physics, vol. 150, 2008.
[16] B.C. McCallum, J.M. Rodenburg, Simultaneous reconstruction of object and aperture functions from multiple far-field intensity measurements, J. Opt. Soc. Am. A 10 (2) (1993) 231–239.
[17] J.R. Fienup, Phase retrieval algorithms: a comparison, Appl. Opt. 21 (15) (1982) 2758–2769.
[18] D.C. Youla, H. Webb, Image restoration by the method of convex projections: part 1—theory, IEEE Trans. Med. Imaging 1 (2) (1982) 81–94.
[19] S. Flåm, J. Zowe, Relaxed outer projections, weighted averages and convex feasibility, BIT Numer. Math. 30 (2) (1990) 289–300.
[20] V. Elser, Phase retrieval by iterated projections, J. Opt. Soc. Am. A 20 (1) (2003) 40–55.
[21] V. Elser, I. Rankenburg, P. Thibault, Searching with iterated maps, Proc. Natl. Acad. Sci. USA 104 (2) (2007) 418–423.
[22] R.D. Millane, Phase retrieval in crystallography and optics, J. Opt. Soc. Am. A 7 (3) (1990) 394–411.
[23] H.H. Bauschke, J.M. Borwein, On projection algorithms for solving convex feasibility problems, SIAM Rev. 38 (3) (1996) 367–426.
[24] V. Elser, Random projections and the optimization of an algorithm for phase retrieval, J. Phys. A Math. Gen. 36 (12) (2003) 2995–3007.
[25] R.W. Gerchberg, W.O. Saxton, A practical algorithm for the determination of phase from image and diffraction plane pictures, Optik 35 (1972) 237–246.
[26] P. Thibault, I. Rankenburg, Optical diffraction microscopy in a teaching lab, Am. J. Phys. 75 (9) (2007) 827–832.
[27] R. Bates, Fourier phase problems are uniquely solvable in more than one dimension. I: underlying theory, Optik 61 (3) (1982) 247–262.
[28] O. Bunk, M. Dierolf, S. Kynde, I. Johnson, O. Marti, F. Pfeiffer, Influence of the overlap parameter on the convergence of the ptychographical iterative engine, Ultramicroscopy 108 (5) (2008) 481–487.